

# Effect of Doping and Morphology on UV Emission in Low-Dimensional ZnO:Na Structures

Benjamin Straube,\* German Bridoux, Cecilia Zapata, Jorge M. Ferreyra, Manuel Villafuerte, Gabriela Simonelli, Pablo Esquinazi, Claudia Rodríguez Torres, and Silvia I. Perez de Heluani\*

**Band-edge photoluminescence of zinc oxide materials reveals a phonon-assisted ultraviolet emission enhanced by Na doping. We report the synthesis of ZnO and Na-doped ZnO, the changes in structure and optical properties as a function of doping concentration and synthesis temperature. The obtained samples are nanoneedles, microparticles, and microwires. The structural effect of Na doping is studied by X-ray diffraction and Raman spectroscopy. Room temperature photoluminescence reveals a contribution of band bending at the surface of the nanostructures, decreasing with Na concentration. Franz–Keldysh effect predicts strong electric field localized in the depletion region and appears to be the cause of red-shift in UV band emission of nanoneedles in comparison to microwires. Our results indicate that Na doping introduces an acceptor level between 150 and 200 meV above the valence band.**

## 1. Introduction


The wide-gap semiconductor zinc oxide is one of the most studied optical semiconductors. There is a large amount of

Dr. B. Straube, Dr. C. Zapata, Prof. J. M. Ferreyra, Dr. M. Villafuerte, Dr. G. Simonelli, Prof. S. P. Heluani  
Laboratorio de Física del Sólido  
Dpto. de Física  
INFINOA (CONICET-UNT)  
Facultad de Ciencias Exactas y Tecnología  
Universidad Nacional de Tucumán  
Av. Independencia 1800, (4000) Tucumán, Argentina  
E-mail: bstraube@herrera.unt.edu.ar; sperez@herrera.unt.edu.ar

Dr. B. Straube, Dr. G. Bridoux, Dr. M. Villafuerte  
Consejo Nacional de Investigaciones Científicas y Técnicas – CONICET, Buenos Aires, Argentina

Prof. P. Esquinazi  
Felix-Bloch-Institute  
Fakultät für Physik und Geowissenschaften  
Linnéstraße 5, 04103 Leipzig, Germany

Prof. C. Rodríguez Torres  
IFLP-CCT- La Plata-CONICET and Dpto de Física  
Facultad de Ciencias Exactas  
Universidad Nacional de La Plata  
C.C. N 67, 1900 La Plata, Buenos Aires, Argentina

 The ORCID identification number(s) for the author(s) of this article can be found under <https://doi.org/10.1002/pssb.201800056>.

DOI: 10.1002/pssb.201800056

literature demonstrating that micro and nano-structures can be easily grown with/ from ZnO. ZnO nanoparticles are attractive for sensing biological structures, solar cells, photocatalysis, and biomedical applications. On the other side, ZnO nano and microwires have been widely studied and used in optoelectronics and nano/micro-electronics as UV nanolasers, field emission devices, photodetectors.<sup>[1]</sup> Moreover, the subject of doping and defect induced properties in ZnO materials have attracted much attention not only due to its technological importance, but also from the point of view of fundamental physics.<sup>[2–7]</sup> In the last years, several groups reported interesting new physical properties at room temperature in ZnO as exciton-polariton formation in high-quality

microcavities and magnetism. However, obtaining high quality ZnO materials with room-temperature specific physical properties in a reproducible way, is a goal not attained yet.<sup>[8–11]</sup> It is widely accepted that for any of its mentioned technological applications, it is crucial to gain further understanding about the role of the native defects, the impurities or dopants in the ZnO physical properties at and beyond room temperature. In this research line, our investigation is particularly motivated by the renewed interest of the role of defects in the observed room temperature magnetic order and in optic and electronic properties.<sup>[12–15]</sup>

Controversial results are found in the literature about the role of native defects on electrical, optical, and magnetic properties of ZnO. It was proposed that oxygen vacancies  $V_O$ , introduce a metastable shallow donor state and are responsible for the color and conductivity in ZnO, while zinc vacancies  $V_{Zn}$  are remarkably unstable.<sup>[2,16]</sup> However, evidence of  $V_{Zn}$  acting as dominant acceptor in *n*-type ZnO was reported in Tuomisto et al.<sup>[17]</sup> Other authors suggest that the *n*-type conductivity of ZnO is due to the incorporation of impurities during growth or annealing, rather than to native point defects.<sup>[18,19]</sup>

Recently theoretical and experimental studies agree that defect induced magnetization in ZnO is promoted by unpaired 2p electrons at O sites surrounding the  $V_{Zn}$ <sup>[12,20,21]</sup> and other authors describe the role of oxygen vacancies in the magnetic order.<sup>[22–24]</sup> Particularly in Li et al.<sup>[22]</sup> the authors describe a strong correlation between the presence of  $V_O$  and saturation

magnetization. Both lines of research argued the need of introduce holes to strengthen magnetism.

In this scene, the main obstacle for room-temperature operation in technological applications is the reproducibility of *p*-type ZnO. In principle this can be achieved through the understanding of the processes involved in doping and growth of the structures. Lee and Chang<sup>[25]</sup> describe a method for fabricating *p*-type ZnO with group-I elements such as Li and Na based on first principles calculations. Their work suggests a way to produce *p*-type magnetic material. In this matter we have reported recently the existence of magnetic order at room temperature in Li-doped ZnO microwires after proton irradiation.<sup>[12]</sup>

In this work, we report the synthesis of undoped ZnO and Na-doped ZnO powders and the systematic characterization of different nano- and microstructures grown during synthesis processes which cover a wide temperature range. The materials obtained are nanoneedles, microparticles, and microwires of both ZnO and Na-doped ZnO. The evolution of the structural and optical properties as a function of doping and growth temperature is fully described in this manuscript.

## 2. Experimental Section

The synthesis process of different ZnO consists in the production of ZnO and Na doped ZnO powders by thermal decomposition of zinc acetate (ZnAc). ZnAc dihydrate  $\text{Zn}(\text{CH}_3\text{COO})_2 \cdot 2\text{H}_2\text{O}$ , and sodium hydroxide mono hydrate  $\text{NaOH} \cdot \text{H}_2\text{O}$  (Sigma-Aldrich 99.99%) were used as starts precursors. These were mixed with deionized water at the nominal concentration of 1–7at% Na/Zn and stirred in ultrasound to obtain a homogeneous solution. After drying at 100 °C and milling, the dehydrated powders were thermally treated using a heating rate shown in Figure 1 and afterwards naturally cooled to room temperature.

This process was done under elevated partial water vapor pressure to ensure the formation of crystalline zinc oxide below 300 °C and to avoid sublimation of ZnAc above 183 °C.<sup>[26]</sup> At this stage (temperature below 300 °C) nano-structures in form of particles and mostly needles were obtained with an average size between 100 and 200 nm in length and 10 nm in diameter, see Figure 2a.

After previously described thermal treatment, the powders were annealed at 900 °C during 1 h in air to obtain microparticles. The average size of obtained particles was 1 μm, Figure 2b.

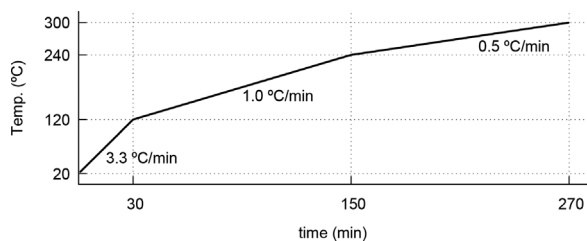


**Figure 1.** Thermal treatment of dehydrate ZnAc powders under elevated partial water vapour pressure.

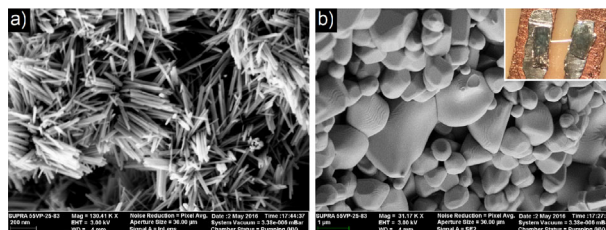


**Figure 2.** a) SEM image of nanoneedles (300 °C). b) SEM image of microparticles (900 °C), inset: a single microwire with electric contacts (indium soldering)  $\approx 0.5$  mm apart.

Thermal analysis studies were made using dta and tga instruments Shimadzu DTA-50 and TG-50 respectively. The experiments were performed between ambient and 800 °C with a heating rate of 10 °C min<sup>-1</sup>. Dry nitrogen as purge gas at a flow rate of 10 ml min<sup>-1</sup> was used.

The obtained microparticles synthesized with different concentrations of Na were used as precursor powders for growing undoped and doped ZnO microwires by carbothermal process, see inset in Figure 2c. In such a synthesis method 200 mg of a pellet compressed at 3Tn of ZnO/graphite (mass ratio of 1:1) was introduced within a quartz tube inside a tubular furnace at 1150 °C during one hour in air at atmospheric pressure.

Nanoneedles (nns), microparticles (mps), and microwires (mws) were labeled as NaZnO-*n*, *n* = 1,3,5,7 corresponding to nominally 1–7at% Na. Representative SEM images of the samples are shown in Figure 2.

The size and morphology of the structures were measured by Scan Electron Microscopy (SEM), the structure and phases by X-ray diffraction (XRD) and by Raman spectroscopy. XRD patterns were recorded by  $\theta - 2\theta$  scans with Cu K $\alpha_1$  and Cu K $\alpha_2$  source radiation.

Photoluminescence (PL) measurements were carried out at room temperature and ambient conditions on nns and on single mws with a 15 mW He–Cd laser from Kimmon Koha Co. using the 325 nm line as the excitation source ( $\approx 0.2$  mm diameter beam spot). The emission was collected in a back-scattering geometry with an AvaSpec-ULS3648 spectrometer.

For photocurrent measurements ohmic electrical contacts, at all measured temperatures, were made with indium soldering. A xenon 1000 W lamp was used for excitation and an Oriel monochromator with estimated flux density of 10  $\mu\text{W cm}^{-2}$  in the UV range. The wavelength sweep rate used to measurements of photoconductance spectra was 0.5 nm s<sup>-1</sup>.

## 3. Results

### 3.1. Structural Characterization

TGA and DTA of ZnAc materials are shown in Figure 3. After dehydration and weight loss around 50 °C all samples were in comparable dry starting point condition. The pronounced weight loss between 200 and 300 °C, present in all samples, shows the thermal decomposition of ZnAc. The narrow endothermic peak at 257 °C agree with ZnAc fusion, and the widest around 298 °C (also endothermic) indicate the end of decomposition. No further weight loss occurs after 300 °C (see DTA curves). The

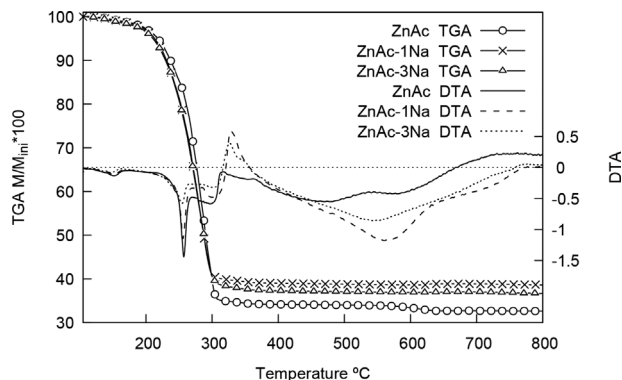


**Figure 3.** Differential thermal analysis (DTA) and thermogravimetric analysis (TGA) of ZnAc and doped ZnAc.

exothermic reaction visible in the dta curves above 300 °C is attributed to crystallization and growth of the nano needles. Between 400 and 750 °C the curve shows an endothermic reaction due to the coalescence of the nano-size material into micro-size particles, see Figure 3.

XRD data, **Figure 4a**, confirms wurtzite structure in all sample and concentrations. No characteristic peaks of any other structure were detected, suggesting that Na doping does not affect the wurtzite structure. The  $c$  values range from  $(5.1918 \pm 0.0001)$  Å to  $(5.2152 \pm 0.0001)$  Å and the parameter  $a$  between  $(3.2349 \pm 0.0001)$  Å and  $(3.2547 \pm 0.0001)$  Å for nns with different concentration of Na, see Figure 4b,c. These results suggest that Na is a substitutional defect in nns, however, it is possible that due to low temperature growth condition, Na atoms were not located in energetically favorable sites (see photoluminescence results in the

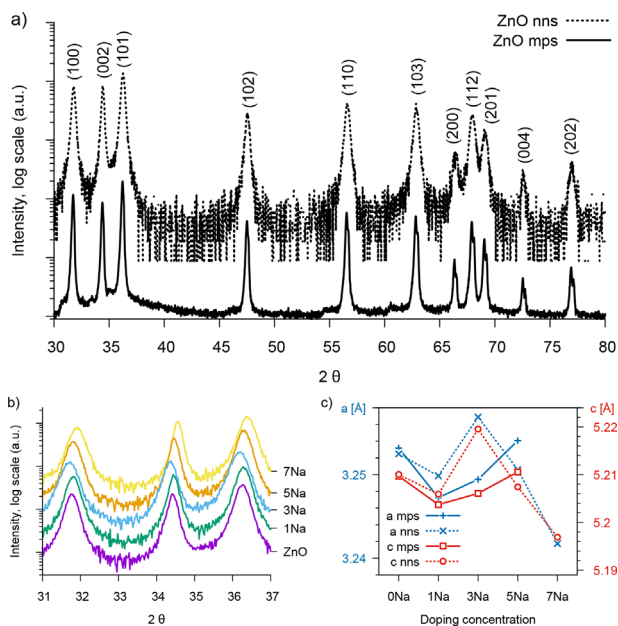


**Figure 4.** a) XRD pattern of representative samples: nanoneedles (dotted) and microparticles (solid). b) XRD pattern of ZnO and doped nanoneedles. The spectra are vertically shifted. c) Lattice parameters  $a$  and  $c$  as a function of Na concentration.

next section). No significant difference in lattice parameters is observed between mps and mws for all Na concentrations. In mws we obtained a mean value of  $(5.2070 \pm 0.0005)$  Å for  $c$  parameter, this lies within the range of previous reported values for ZnO wurtzite ( $c = 5.2042 - 5.2075$  Å). For parameter  $a$  the mean value obtained for mws is  $(3.2509 \pm 0.0005)$  Å close to reported value  $3.2475 - 3.2501$  Å. The ratio  $c/a$  obtained for mps and mws is 1.604, which is also consistent with the values given in the literature for crystalline bulk  $1.503 - 1.6035$ .<sup>[27]</sup>

Room temperature micro Raman spectroscopy was performed with  $\lambda_{exc} = 532$  nm for NaZnO-5 and NaZnO-1 nns, mps, and nws. **Figure 5** shows the obtained spectra of representative NaZnO-5 samples, normalized to the intensity of the E2 (low) mode. Spectra of NaZnO-1 structures (not shown) did not present any significant difference with those of Figure 5, without shifting in any of the peaks. All the spectra present two dominant peaks at  $99$  and  $439$   $\text{cm}^{-1}$  corresponding to E2 (low) and E2 (high) Raman active modes characteristics of the wurtzite phase of ZnO. These are the only well-defined peaks in the case of nns probably due to random orientation in the configuration set up. A1(TO) at  $378$   $\text{cm}^{-1}$  and E1(TO) at  $409$   $\text{cm}^{-1}$  are important in mws spectrum because of the preferred direction of incident light with respect to the  $c$  axis of mw (perpendicular to  $c$ ). Also, some multiphonon peaks appear at  $202$ ,  $331$ ,  $484$ , and  $541$   $\text{cm}^{-1}$ .<sup>[28]</sup> A1(LO) and E1(LO) overlap near  $580$   $\text{cm}^{-1}$  possibly due to modes induced by surface defects such as oxygen vacancies.<sup>[29]</sup> Na doping does not introduce new modes neither significant peaks shift, strengthening the argument for a substitutional doping.

### 3.2. Photoluminescence and Photoconductivity

Room temperature photoluminescence of undoped and doped nanoneedles and microwires shows two bands, one above 3.0 eV, attributed to the excitonic emission and the second band around 2.4 eV corresponds to deep levels emission. This latter covers the visible spectral regions. The PL spectra normalized by the 2.4 eV emission of nns and mws are shown in **Figure 6a,b** respectively. The results exhibit higher emission in the blue band compared to the green one for doped and undoped nanoneedles. The same behavior is observed for 3% and 5% Na doped mws.

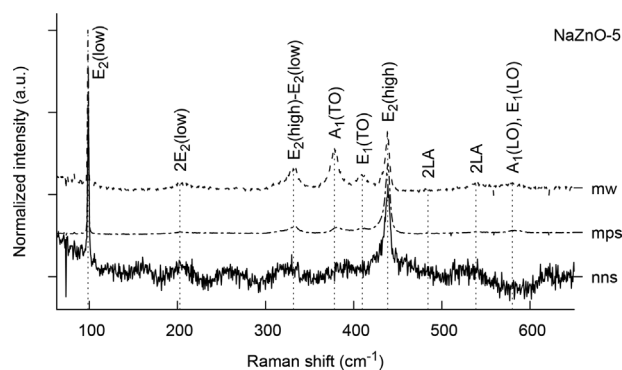


**Figure 5.** Raman spectra of representative NaZnO-5 samples, normalized to the intensity of the E2 (high) mode.

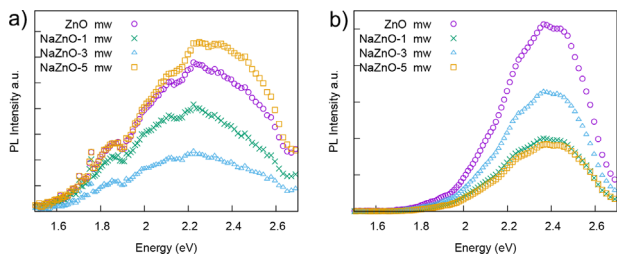


**Figure 6.** Normalized PL spectra of ZnO and doped ZnO samples, a) nanoneedles, b) single microwires.

The NaZnO-5 doped mws has UV intensities six times larger than the green emission.

Figure 7a,b show the deep levels pl emission band for nns and mws respectively. Although 3% and 1% Na doping nns show a reduction of the deep level emission compared to undoped ones, 5% Na doped nns has an increase. This lack of systematics suggests that at low temperatures Na doping did not reach their thermodynamic equilibrium state, in agreement with XRD results. On the other side, deep level PL band measured in mws shows a systematic decrease of intensities with Na doping. Beside controversy,<sup>[18]</sup> native defects have been suggested as a potential source of the green luminescence band. Also, the difficulties for *p*-type doping have been attributed to the compensation by native point defects.<sup>[30]</sup> Figure 7b indicates that Na doping produces a decrease, or passivation, of native defects in the ZnO mws.

It was reported that the native defect, particularly oxygen vacancies, are the dominant factor for emission near 2.4 eV and also are responsible for the slow decay of photoconductivity.<sup>[31]</sup> Another evidence of relative concentration of deep level defects, in undoped and doped mws, could be attained from their effect over a faster or slower carrier recombination mechanisms in measurements of photoresistance relaxation. If deep donor levels act as electron trapping, they will have an important influence on the recombination kinetic. Trapping centers make experimentally observed photocurrent decay time longer than free carrier lifetime.

Although all Na doped mws are insulators in darkness, they have a great sensitivity to light, and it is possible to measure transient relaxation curves of photoresistance after illumination is turned off. Figure 8 shows a logarithmic plot of transient relaxation of normalized photoresistance  $(R(t) - R_0)/R_0$ , as a function of time of undoped and Na doped mws.  $R_0$  is the photoresistance value just before the illumination is removed. Lower kinetic recombination

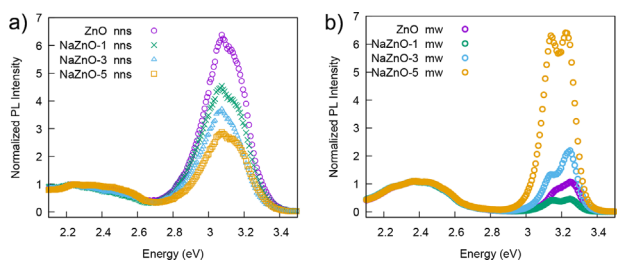


**Figure 7.** Normalized deep level PL band of ZnO and doped samples, a) nanoneedles, b) single microwires.

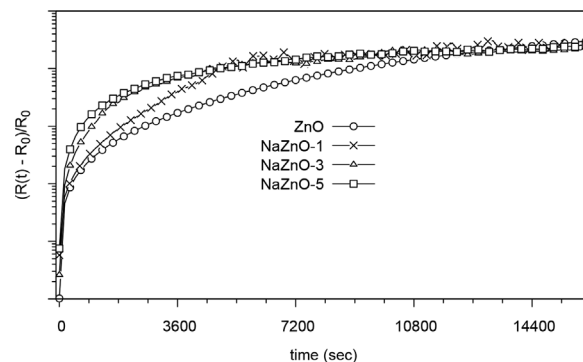


**Figure 8.** Normalized photoresistance as a function of the time of undoped and Na-doped microwires.

of ZnO sample compared with Na doped mws can be seen in Figure 8 in the region before saturation value and shows a systematic behavior with Na concentration.

In order to obtain additional information about characteristics energies we perform measurements of photoresponse (PR) in selected mws. PR spectra of ZnO and 5% Na doped mws are shown in Figure 9 in superposition of pl result. PR is defined as  $PR = (C_{h\nu} - C_d)/C_d$ ,  $C_{h\nu}$  is the conductance under illumination with photon of energy  $h\nu$  and  $C_d$  is the dark conductance. Before starting the experiments we reach the saturation value in dark. Figure 9 shows that mws are not sensible at photon energy between 1.9 and 2.8 eV. The PR measurements shows that the photocurrent increases three orders of magnitude in Na doped mws respect to undoped samples.

## 4. Discussion

In PL spectra of nns we can highlight two features: the shift of  $\approx 0.1$  eV toward lower energies of the UV band and the widening of this band respect to that of mws, see Figure 6a,b. This latter effect is larger for undoped samples. Both effects can be explained due to a large contribution of band bending at the surface of nns and their sizes dispersion. The band bending gives rise to a tail in the density of states below the gap due to the effect of an electric field on the optical absorption coefficient. The electric field is induced by the local fields of charged impurities.

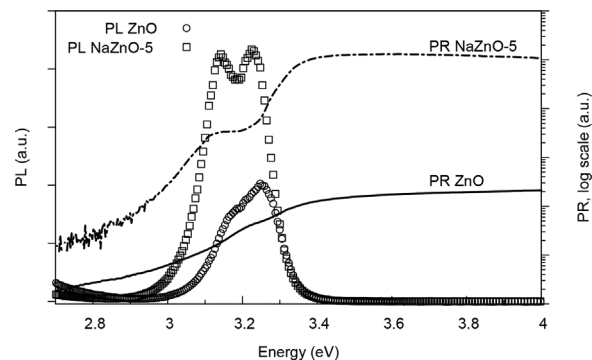


**Figure 9.** PR and PL measured in ZnO and NaZnO-5 microwires.

This effect is described by Franz–Keldysh in a theory of the photon-assisted tunneling and predicts that the internal fields produce an effective band gap reduction which is the lower limit of the tail size of the density of states below the gap.<sup>[32,33]</sup> The diameter of nns is between 10 and 30 nm, then the depletion region in the band structure covers much of the volume of nano-needles i.e., it is completely depleted.

Considering cylindrical geometry and using the relation between diameter and the induced electric field, the estimated value is  $\xi = 2 \times 10^7 \text{ V m}^{-1}$  for a mean diameter of 20 nm.<sup>[34]</sup> The band tail width  $\Delta E$  from the edge of the conduction band is calculated using

$$\Delta E = \frac{\hbar^2}{2 \cdot m_{\text{eff}}} \left( \frac{3}{4} \cdot e \cdot \xi \frac{2 \cdot m_{\text{eff}}}{\hbar^2} \right)^{2/3} \quad (1)$$

Here  $\xi$ ,  $m_{\text{eff}}$ ,  $e$ ,  $\hbar$  are the electric field, effective mass, electron charge, and Planck constant ( $\hbar/2\pi$ ), respectively. The value obtained for  $\Delta E$  is 31 meV. The Below-gap optical absorption coefficient  $\alpha(w)$  as a function of the field (Franz–Keldysh effect) is written as,

$$\alpha(\omega) = \frac{\alpha_b}{32 \cdot \pi^2 E_g - \hbar\omega} \xi e^{-\frac{4}{3\kappa} \left( \frac{2 \cdot m_r (E_g - \hbar\omega)}{\hbar^2} \right)^{3/2}}$$

$\alpha_b$  is a function of the optical dipole matrix element. The energy below the gap for which  $\alpha(\omega) = 0.1$ ,  $E_g - \hbar\Omega = 1.74 \cdot \Delta E$ . Then the gap was reduced by  $1.74 \times 31 \text{ meV} = 54 \text{ meV}$ .

On the other side, the width of the UV band of nns decreases smoothly and systematically with Na concentration due to the shift of the lower energy edge toward higher energies (the higher energy edge remains almost fixed), see Figure 6a. Yang et al.<sup>[35]</sup> using density functional theory obtained an attractive interaction between  $\text{Na}_{\text{Zn}}$  and  $\text{V}_{\text{O}}$ . The latter could lead to a decrease in the amount of oxygen vacancies near the surface which could be the source of surface charge which generates the band bending thereby causing the decrease of gap reduction.<sup>[36]</sup>

The UV bands of mws, Figure 6b, are all shifted toward larger energy than nns bands, and they are also narrower. The mws PL reveals exciton emission in the UV band.

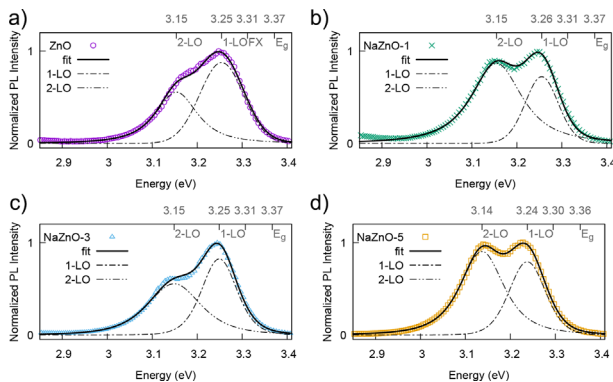


**Figure 10.** Deconvolution of the UV band of one single microwire, a) undoped ZnO, b) NaZnO-1, c) NaZnO-3 and d) NaZnO-5. The data are normalized at maximum UV intensity.

**Figure 10a–d** shows the fitting curves for UV band of ZnO, NaZnO-1, NaZnO-3, and NaZnO-5 mws. The spectra are resolved by means of two  $FS$  functions (Eq. 2) described by Frazer and Suzuki.<sup>[37]</sup>

$$FS(\epsilon, T) = a \left[ 1 + \left( 2^{fs^2} - 1 \right) \left( 2 \cdot (\epsilon - b) / c \right)^2 \right]^{(fs^{-2})}, \quad (2)$$

where  $a$ ,  $\epsilon$ , and  $c$  are fitting parameters: maximum height, the peak position and full width at half maximum, respectively.  $fs$  is a shape factor between 0 and 1. The parameter  $b$  has a temperature dependence, corresponding to each peak, of the form

$$\text{FX: } b = \epsilon_0 + k_B T, \quad (3)$$

$$(1\text{-LO}): b = \epsilon_0 - \hbar\omega_0 + 3/2 \cdot k_B T, \quad (4)$$

$$(2\text{-LO}): b = \epsilon_0 - 2\hbar\omega_0 + 1/2 \cdot k_B T, \quad (5)$$

$\epsilon_0$  is the absorption line energy of the FX at  $T=0$  and  $\hbar\omega_0$  is the phonon energy delivered by the free exciton in a scattering process. Eqs. (4) and (5), express that the photoluminescence line of the first and second phonon replica are shifted, with respect to the FX, toward lower energies by a multiple of the phonon energy  $\hbar\omega_0$ . The last term in Eqs. (3), (4), and (5) consider the kinetic energy of the exciton. The fit shows no contribution of the FX but of first and second phonon replica 1-LO and 2-LO to the luminescence at room temperature. The adjustments in Figure 10 were made considering a separation of  $\hbar\omega_0 = 72 \text{ meV}$  between all replicas. The upper  $x$ -axis shows energies values calculated using Eqs. (3)–(5). The gap energy value is obtained from the fit, and is estimated in 3.37 eV at zero temperature using  $E_g(T) = \epsilon_0 + k_B T + E_x$  where  $E_x = 0.060 \text{ eV}$  is the exciton energy. The peaks resolved at 3.25 and 3.15 eV corresponds to 1-LO and 2-LO, respectively, FX is estimated at 3.31 eV. These results are consistent with values reported in the literature. Also from the fitting we observed that the peaks intensities of the 2-LO replica are larger respect to the first phonon replica in Na doping mws, and the difference is enhanced with Na concentration, suggesting a contribution due to a bound exciton (BX) replica or, a donor acceptor pair (DAP) emission. This contributions are not added to the fits. Considering this latter argument and taken into account that the Free Acceptor energy  $E_{FA}$  have already been measured at higher energies,<sup>[38]</sup> we can estimate an acceptor binding energy (EA) using a DAP energy  $\approx 3.15 \text{ eV}$ , and the expression<sup>[39]</sup>:

$$EA = E_g - E_D - \left( E_{DAP} - \alpha N_D^{1/3} \right),$$

where  $E_g$ ,  $E_D$ ,  $E_{DAP}$ , and  $N_D$  are intrinsic band gap, donor binding energy, DAP emission energy position and concentration of donor defects, respectively,  $\alpha = 2.7 \times 10^{-8} \text{ eV cm}$ . We obtain  $EA \approx 150 \text{ meV}$  for  $N_D$  between  $10^{14}$  and  $10^{16} \text{ cm}^{-3}$  and  $E_D = 0.04 \text{ eV}$ .

In the overlap between photocurrent (which is directly related to optical absorption coefficient) and photoluminescence UV band (Figure 9), measurements in Na doped sample show a clear

quenching of photocurrent (the plateau) that occurs coincident with the range of exciton peaks and is released afterwards. This quenching is not observed in undoped samples and is an indicative that the exciton emission has contributions of an acceptor level associated to Na doping. Taken into account our experimental evidence we suggest that Na doping introduces an acceptor level 150–200 meV above the valence band.

## 5. Conclusions

In summary, we describe the synthesis of nano and micro structures of Na-doped ZnO. UV band emission shift to lower energies of the nano structures is explained as a consequence of Franz–Keldysh effect. In doped samples, the electron concentration is lower in the surface mainly due to a decrease in the amount of oxygen vacancies near the surface and an increase of holes associated to Na acceptor states, thus decreasing the Franz–Keldysh effect. Our results show that doping has little influence in optical properties of low-temperature synthesized nano structures. But in micro structures a strong and stable room temperature exciton–photon coupling and a phonon-assisted UV emission is enhanced by doping with Na. Our experimental results indicate that Na doping introduces an acceptor level 150–200 meV above the valence band and that doped ZnO microwires are promising semiconductor structures for the realization of room-temperature blue/UV optoelectronics.

## Acknowledgements

The authors thank Professor Fernando Ikawa for their assistance during the Raman measurements at the Instituto de Física Gleb Wataghin, Campinas-SP, Brazil. This work was partially supported by PIP- No. 585, SCAIT-26/E530, PICT-3356 (Argentina), and the SFB762 (Germany). P.D. E. acknowledges the support of the program RAICES and the Milstein Fellowship MINCYT (Argentina). We appreciate financial support by LNLS, Campinas, SP, Brazil (proposals PGM 20160571).

## Conflict of Interest

The authors declare no conflict of interest.

## Keywords

microparticles, microwires, nanoneedles, Na-doping, photoluminescence, photoresponse, ZnO

Received: February 9, 2018  
Revised: April 28, 2018  
Published online:

- [1] C. F. Klingshirn, B. K. Meyer, A. Waag, A. Hoffmann, J. Geurts, *From Fundamental Properties Towards Novel Applications*. Springer Series in materials science, Springer, Berlin, Heidelberg **2010**.
- [2] S. Lany, A. Zunger, *Phys. Rev. Lett.* **2007**, *98*, 045501.
- [3] K. Jindal, M. Tomar, R. Katiyar, V. Gupta, *AIP Adv.* **2015**, *5*, 027117.
- [4] L. Sponza, J. Goniakowski, C. Noguera, *Phys. Rev. B* **2016**, *93*, 195435.
- [5] T. Kinoshita, H. Ishihara, *Phys. Rev. B* **2016**, *94*, 045441.
- [6] A. Sundaresan, R. Bhargavi, N. Rangarajan, U. Siddesh, C. N. R. Rao, *Phys. Rev. B* **2006**, *74*, 161306.
- [7] M. Zamfirescu, A. Kavokin, B. Gil, G. Malpuech, M. Kaliteevski, *Phys. Rev. B* **2002**, *65*, 161205.
- [8] H. Peng, H. J. Xiang, S. H. Wei, S. S. Li, J. B. Xia, J. Li, *Phys. Rev. Lett.* **2009**, *102*, 017201.
- [9] D. C. Look, B. Claflin, *Phys. Status Solidi B* **2004**, *241*, 624.
- [10] M. D. McCluskey, S. J. Jokela, *J. Appl. Phys.* **2009**, *106*, 071101.
- [11] J. B. Yi, C. C. Lim, G. Z. Xing, H. M. Fan, L. H. Van, S. L. Huang, K. S. Yang, X. L. Huang, X. B. Qin, T. W. U Wang, H. T. Zhang, X. Y. Gao, T. Liu, A. T. S. Wee, Y. P. Feng, J. Ding, *Phys. Rev. Lett.* **2010**, *104*, 137201.
- [12] I. Lorite, B. Straube, H. Ohldag, P. Kumar, M. Villafuerte, P. Esquinazi, C. E. Rodríguez Torres, S. Perez, D. E. Heluani, V. N. Antonov, L. V. Bekenov, A. Ernst, M. Hoffmann, S. K. Nayak, W. A. Adeagbo, G. Fischer, W. Hergert, *Appl. Phys. Lett.* **2015**, *106*, 082406.
- [13] B. Dolgin, I. Lorite, Y. Kumar, P. Esquinazi, G. Jung, B. Straube, S. P. De Heluani, *Nanotechnology* **2016**, *27*, 305702.
- [14] M. Villafuerte, D. J. Zamora, G. Bridoux, J. M. Ferreyra, M. Meyer, S. P. Heluani, *J. Appl. Phys.* **2017**, *121*, 064501.
- [15] J. Ferreyra, G. Bridoux, M. Villafuerte, B. Straube, J. Zamora, C. Figueroa, S. Heluani, *Solid State Commun.* **2017**, *257*, 42.
- [16] L. Liu, Z. Mei, A. Tang, A. Azarov, A. Kuznetsov, Q. K. Xue, X. Du, *Phys. Rev. B* **2016**, *93*, 235305.
- [17] F. Tuomisto, V. Ranki, K. Saarinen, D. C. Look, *Phys. Rev. Lett.* **2003**, *91*, 205502.
- [18] A. Janotti, C. G. V. De, *Rep. Prog. Phys.* **2009**, *72*, 126501.
- [19] D. M. Hofmann, A. Hofstaetter, F. Leiter, H. Zhou, F. Henecker, B. K. Meyer, S. B. Orlinskii, J. Schmidt, P. G. Baranov, *Phys. Rev. Lett.* **2002**, *88*, 045504.
- [20] Q. Wang, Q. Sun, G. Chen, Y. Kawazoe, P. Jena, *Phys. Rev. B* **2008**, *77*, 205411.
- [21] P. Esquinazi, W. Hergert, D. Spemann, A. Setzer, A. Ernst, *IEEE Trans. Magn.* **2013**, *49*, 4668.
- [22] F. Li, X. C. Liu, R. W. Zhou, H. M. Chen, S. Y. Zhuo, E. W. Shi, *J. Appl. Phys.* **2014**, *116*, 243910.
- [23] M. Zhu, Z. Zhang, M. Zhong, M. Tariq, Y. Li, W. Li, H. Jin, K. Skotnicova, Y. Li, *Ceram. Int.* **2016**, *43*, 3166.
- [24] S. Katba, S. Jethva, M. Udeshi, P. Trivedi, M. Vagadia, D. Shukla, R. Choudhary, D. Phase, D. Kuberkar, *Appl. Surf. Sci.* **2017**, *423*, 100.
- [25] E. C. Lee, K. J. Chang, *Phys. Rev. B* **2004**, *70*, 115210.
- [26] T. Arii, A. Kishi, *Thermochim. Acta* **2003**, *400*, 175.
- [27] U. Özgür, Y. I. Alivov, C. Liu, A. Teke, M. A. Reshchikov, S. Dogan, V. Avrutin, S. J. Cho, H. Morko, *J. Appl. Phys.* **2005**, *98*, 041301.
- [28] R. Cuscó, E. Alarcón-Lladó, J. Ibáñez, L. Artús, J. Jiménez, B. Wang, M. J. Callahan, *Phys. Rev. B* **2007**, *75*, 165202.
- [29] A. Pradhan, K. Zhang, G. B. Loutts, U. N. Roy, Y. Cui, A. Burger, *J. Phys.: Condens. Matter* **2004**, *17*, 7123.
- [30] Y. Tsur, I. Riess, *Phys. Rev. B* **1999**, *60*, 8138.
- [31] S. B. Zhang, S. H. Wei, A. Zunger, *Phys. Rev. B* **2001**, *63*, 075205.
- [32] W. Franz, *Photon-Assisted Tunneling (Franz-Keldysh Effect)*. Springer US, Boston, MA **1969**, pp. 207.
- [33] L. V. Keldysh, *Sov. Phys. JETP* **1958**, *7*, 788.
- [34] A. Cavallini, L. Polenta, M. Rossi, T. Stoica, R. Calarco, R. J. Meijers, T. Richter, H. Lüth, *Nano Lett.* **2007**, *7*, 2166.
- [35] X. P. Yang, J. G. Lu, H. H. Zhang, B. Lu, J. Y. Huang, C. L. Ye, Z. Z. Ye, *J. Appl. Phys.* **2012**, *112*, 113510.
- [36] Y. Y. Tay, T. T. Tan, M. H. Liang, F. Boey, S. Li, *Phys. Chem. Chem. Phys.* **2010**, *12*, 6008.
- [37] R. D. B. Fraser, E. Suzuki, *Anal. Chem.* **1969**, *41*, 37.
- [38] D. C. Look, D. C. Reynolds, C. W. Litton, R. L. Jones, D. B. Eason, G. Cantwell, *Appl. Phys. Lett.* **2002**, *81*, 1830.
- [39] S. Pal, T. Rakshit, S. Singha, K. Asokan, S. Dutta, D. Jana, A. Sarkar, *J. Alloys Compd.* **2017**, *703*, 26.